Energy Engineering

Tech Science Press

https://doi.org/10.32604/ee.2026.076966

ARTICLE

Modeling and Optimization of Air Staging in an Ammonia-Fueled Gas Turbine Combustion Chamber

Serhiy Serbin[1,*], Bohdan Lychko[2] and Kateryna Burunsuz[1]

[1]Department of Turbine, Admiral Makarov National University of Shipbuilding, Mykolaiv, Ukraine
[2]Department of Operation of Marine Power Plants and Thermal Engineering, Admiral Makarov National University of Shipbuilding, Mykolaiv, Ukraine

*Corresponding Author: Serhiy Serbin. Email: serhiy.serbin@nuos.edu.ua

Received: 30 November 2025; Accepted: 03 February 2026; Published: 27 April 2026

ABSTRACT: This study investigates the use of ammonia as a carbon-free fuel for gas turbines in decarbonized hybrid energy systems. The objective is to predict the emission characteristics of a gas turbine combustion chamber operating on gaseous ammonia by employing detailed combustion kinetics. The chamber is modeled as a network of chemical reactors to simulate the primary reaction zone and the secondary air-mixing zone. The model is based on solving mass and energy conservation equations for chemically reacting flows. Four high-temperature ammonia oxidation mechanisms, comprising 71 to 286 chemical reactions, were used as kinetic schemes. New data were obtained on flame propagation, temperature distributions, and concentrations of stable species at the burner outlet. Calculations were performed for a pressure of 2.0 MPa and an air excess coefficient ranging from 2.36 to 3.55. The dependencies of toxic emissions on ammonia mass flow rate were demonstrated. The results apply to the practical development of gas turbine engines for decarbonized hybrid energy systems.

KEYWORDS: Ammonia; combustion chamber; decarbonization; emission; gas turbine engine

1 Introduction

Ammonia (NH_3) is gaining attention as an alternative fuel for gas turbine applications, owing to its favorable energy storage properties, ease of liquefaction, and potential integration with current fuel supply chains. It presents a notable advantage for decarbonization efforts, as its combustion process releases no carbon dioxide (CO_2). Nevertheless, several key technical and environmental hurdles must be overcome for its practical adoption. The primary challenges encompass:

1. Low flame speed—Ammonia burns considerably slower than conventional fuels like methane or kerosene, posing a risk to combustion efficiency and flame stability in turbines.
2. Nitrogen oxide emissions—Ammonia combustion results in the formation of a significant amount of environmentally harmful nitrogen oxides. Reducing these emissions requires advanced purification systems, such as selective catalytic reduction (SCR).
3. Stable combustion issues—Ensuring stable combustion, particularly during startup or at partial loads, poses significant difficulties.
4. Material compatibility—Ammonia is a chemically aggressive substance, requiring the selection of special materials for combustion chambers and other engine components.

5. Toxicity and safety—Although ammonia can be stored in liquid form at relatively low pressure, it is a toxic and hazardous substance.

The incorporation of ammonia into gas turbine fuel systems entails substantial technological adaptation, particularly with respect to combustion chamber configuration and the implementation of effective nitrogen oxide mitigation strategies. Achieving reliable ammonia-based operation requires coordinated experimental and engineering efforts aimed at enhancing combustion completeness, limiting adverse environmental effects, and maintaining acceptable thermal and mechanical durability of critical components.

Driven by stringent decarbonization targets and the global commitment to reducing pollutant emissions, the energy sector is increasingly investigating ammonia as a promising alternative energy vector. Owing to its high hydrogen content, ammonia represents a viable medium for both hydrogen storage and energy conversion in power generation applications [1,2]. As the worldwide shift toward low-carbon technologies accelerates, ammonia is being actively evaluated as a substitute for conventional fossil fuels [3,4]. In this context, improving overall process efficiency and integrating ammonia synthesis with renewable energy sources are key conditions for achieving carbon-neutral deployment.

One extensively studied pathway involves the co-firing of ammonia with conventional fuels. Experimental investigations have confirmed the technical feasibility of ammonia co-combustion with natural gas in various thermal systems, including gas turbine units [5,6]. However, the intrinsically low chemical reactivity of ammonia imposes limitations on flame stability, often necessitating the addition of more reactive fuels such as methane or hydrogen to facilitate ignition and sustain combustion [7,8]. While effective, this approach increases system complexity and may diminish some of the logistical and environmental advantages associated with the direct use of ammonia.

Alternative concepts focus on modifying ammonia combustion behavior through direct hydrogen enrichment [9,10] or via thermochemical cracking processes that produce hydrogen *in situ* from ammonia [11]. Several studies have investigated the minimum hydrogen content required to maintain stable combustion in spark-ignition engines and internal combustion systems, identifying optimal ammonia–hydrogen mixtures that enhance efficiency and operational robustness [12,13].

A major constraint in ammonia-fueled combustion systems is the significant formation of nitrogen oxides during oxidation [14]. Although a range of ammonia–air combustion strategies has been proposed [15], further refinement is necessary to achieve a balanced combination of low emissions and high thermal efficiency. Despite the long-standing industrial experience with ammonia production, storage, and transport, its combustion behavior remains incompletely understood and continues to attract intensive research attention [16]. Previous investigations [17,18] indicate that the elevated pressures characteristic of gas turbine combustors reduce ignition delay but simultaneously lower laminar flame speeds and promote increased NO_x formation. To mitigate these competing effects, staged combustion concepts have been developed and shown to substantially reduce nitrogen oxide emissions [19]. Moreover, several industrial demonstrations have confirmed the operational feasibility of gas turbines operating on pure ammonia [20].

Additional enhancements in ammonia combustion performance can be achieved by increasing swirl intensity and turbulence within the combustor. These measures improve fuel–air mixing, extend effective residence times, and partially offset the slow reaction kinetics of ammonia. Recent studies [21,22] have explored advanced two-stage combustor designs and low-emission operating regimes specifically optimized for ammonia–air mixtures. Complementary investigations [5,23,24] have addressed ammonia pre-cracking to hydrogen–nitrogen mixtures, numerical simulation of ammonia combustion in dry low-emission systems, and the application of staged combustion techniques for emission control.

A comprehensive overview of recent progress in turbulent ammonia combustion is presented in [25], contributing to both fundamental understanding and applied combustor development. In parallel, study [26] proposes a reduced chemical kinetic mechanism comprising 19 species and 83 reactions for NH_3/H_2 mixtures, enabling the analysis of NO_x formation as a function of combustor operating parameters. The results indicate that increasing inlet pressure can significantly suppress pollutant formation, particularly under fuel-rich conditions. Numerical work in [27] further examines ammonia–hydrogen combustion in a multi-stage combustor using a chemical reactor network (CRN) methodology that combines perfectly stirred, plug-flow, and partially stirred reactor models.

To further enhance ammonia ignition and flame stability, low-temperature plasma-assisted combustion has been proposed [28,29]. Plasma generation techniques based on various discharge methods [30–32], already applied in energy systems [33–35], provide localized energy input that accelerates chemical kinetics. However, their implementation requires modifications to combustor architecture to accommodate plasma–chemical interaction zones.

Despite substantial progress, the application of ammonia as a primary fuel in gas turbine engines continues to face unresolved challenges. Recent reviews of ammonia combustion in gas turbines identify persistent issues related to its physicochemical properties, including reduced combustion efficiency at elevated pressures, susceptibility to flame instability and blow-off at high flow velocities, and the formation of substantial nitrogen oxide emissions.

Conventional NO_x mitigation techniques, such as selective catalytic reduction, may be impractical for high-temperature gas turbine applications due to cost and operational constraints. Therefore, integrating alternative strategies directly within the combustion process is necessary. One promising approach involves staged air distribution along the flame tube to enhance combustion efficiency and minimize NO_x formation.

This study focuses on reducing NO_x emissions in an ammonia-fueled gas turbine combustion chamber by optimizing staged air injection along the length of the flame tube. The novelty of the approach is the complex variation of the air distribution along the length of the high-intensity combustion chamber, supplied, respectively, through the vane swirler, the first and second rows of front device holes, radial primary air injection holes, and radial secondary air injection holes.

2 Materials and Methods

2.1 Combustion Chamber Diagram

In the initial phase of transitioning gas turbine engines from hydrocarbon fuels to ammonia, it is crucial to investigate stable combustion characteristics within high-intensity combustion chambers. Additionally, an early evaluation of pollutant emissions and exhaust gas temperature is necessary.

For this study, a conventional diffusion-type combustion chamber has been selected, as it is adaptable to both liquid and gaseous hydrocarbon fuels in standard configurations.

To analyze the potential for reducing nitrogen oxide emissions through staged primary and secondary air injection along the length of the flame tube, a combustion chamber scheme of a 25 MW gas turbine engine [36] was selected (Fig. 1).

To enable ammonia combustion, the engine's compressor mass airflow rate is maintained, while the ammonia supply to the combustion chamber is determined based on a stoichiometric ratio of L_0 = 6.0466. This value is considerably lower than those of hydrocarbon fuels, which typically range between L_0 = 14.7 and 16.5.

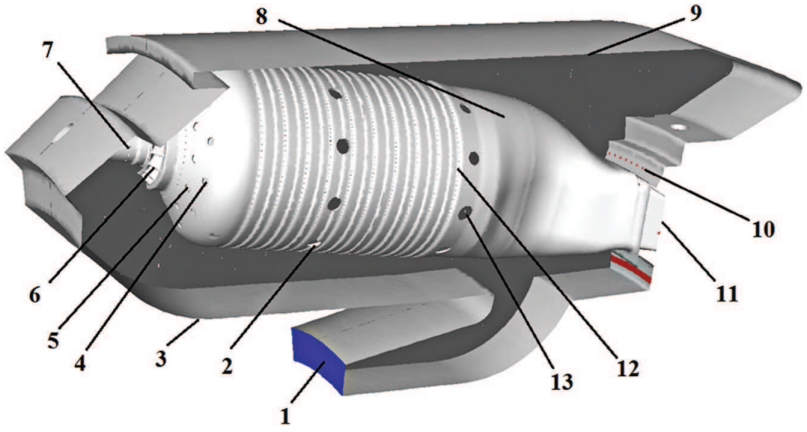

Figure 1: Virtual model of the combustion chamber: 1—air supply after the compressor; 2—radial primary air injection holes; 3—inner casing; 4—second row of front device holes; 5—first row of front device holes; 6—swirler blades; 7—fuel injector; 8—flame tube; 9—outer casing; 10—cooling air supply holes for turbine blade apparatus; 11—combustion products supply to the turbine; 12—flame tube cooling holes; 13—radial secondary air injection holes.

2.2 Mathematical Modeling

To estimate the emission characteristics of a gas turbine engine combustion chamber fueled by ammonia, we adopt the methodology outlined in [34,35], where the chamber is represented as an assembly of distinct chemical reactors.

A homogeneous reactor (HR), also known as a perfectly stirred reactor, assumes complete uniformity of process parameters across the entire reactor volume. A plug flow reactor (PFR), or ideal displacement reactor, models reactant movement in a piston-like manner, leading to concentration and temperature gradients influenced by reaction kinetics and associated physical effects. An adiabatic mixer (AM) functions solely to blend components without triggering chemical reactions.

Fig. 2 illustrates the developed reactor-based model for an ammonia-fueled combustion chamber. The reactors simulate key processes, including combustion in the primary zone, dilution, and secondary air mixing in designated regions.

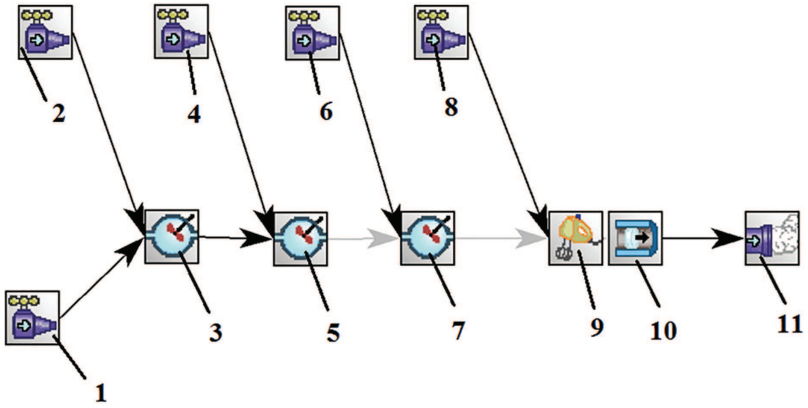

Figure 2: Reactor model of the gas turbine engine combustion chamber operating on ammonia: 1—ammonia injection; 2—air injection through the swirl device; 3—HR1 of the swirl zone; 4—air injection through the front-end device; 5—HR2 of the front-end device; 6—primary air injection; 7—HR3 of the primary zone; 8—secondary air injection; 9—AM; 10—PFR of the mixing zone; 11—combustion chamber outlet.

The homogeneous reactors HR1–HR3 are used to describe successive stages of ammonia oxidation and combustion taking place in the swirl region, the front-end device, and the primary zone of the flame tube, respectively. The reaction products formed in HR1 and HR2 are subsequently directed into HR3, where additional ammonia conversion occurs due to the introduction of air through the first row of radial ports in the flame tube.

Downstream of this section, the reacting mixture enters an adiabatic mixing unit, in which it is combined with secondary air supplied through the second set of radial holes, assuming negligible heat transfer. The dilution and final mixing processes occurring in the flame tube are represented by a plug-flow reactor, which accounts for the coupled chemical and physical transformations of the gas mixture in this region.

The mathematical formulation adopted for the various reactor elements of the combustion chamber model is outlined below. Homogeneous reactors are described using the conservation equations of mass and energy for a chemically reacting flow. Although real combustors employ complex geometries and multiple inlet–outlet arrangements to enhance mixing efficiency, these effects are represented in an idealized manner. Under this assumption, the temperature and species composition within the reactor volume are uniform and equal to the outlet values, while the total mass flow rate through each reactor remains constant.

The governing equations describing the processes in the reactors under consideration, as well as the numerical methods used to solve the systems of chemical kinetics equations, are described in detail in [37–39].

Consider a chemically reacting system comprising I elementary reactions (reversible or irreversible) among K distinct species. The general stoichiometric form for any reaction i is:

$$\sum_{k=1}^{K} \upsilon'_{ki} \chi_k \Leftrightarrow \sum_{k=1}^{K} \upsilon''_{ki} \chi_k, \tag{1}$$

where υ_{ki} are the coefficients of reactants and products, respectively; χ_k is the k-th chemical specie.

The overall rate of formation or depletion of species k is obtained by superposing the contributions of all reactions in which it participates, yielding:

$$\dot{\omega}_k = \sum_{i=1}^{I} \upsilon_{ki} q_i, \tag{2}$$

where $q_i$is the progress rate of the i-th chemical reaction; $\upsilon_{ki} = \left(\upsilon''_{ki} - \upsilon'_{ki}\right)$.

The reaction rate term q_i is computed as:

$$q_i = k_{fi} \prod_{k=1}^{K} [X_k]^{\upsilon'_{ki}} - k_{ri} \prod_{k=1}^{K} [X_k]^{\upsilon''_{ki}}, \tag{3}$$

where k_{fi}, k_{ri} are the forward and backward rate constants, respectively; $[X_k]$ is the volumetric concentration of species k.

The forward reaction rate constant is described using an Arrhenius-type formulation:

$$k_{fi} = A_i T^{\beta_i} \exp\left(\frac{-E_i}{RT}\right), \tag{4}$$

where A_i is the pre-exponential factor; β_i is the temperature exponent; E_i is the activation energy; R is the universal gas constant, and T is the absolute temperature.

A comprehensive mathematical description of all reactor types in the combustion chamber model is available in [39]. This study analyzed the combustion process using four detailed ammonia oxidation mechanisms: Scheme 1 by Xiao et al. [40] (71 reactions, 23 species), Scheme 2 by Stagni et al. [41] (203 reactions, 31 species), Scheme 3 by Li et al. [42] (160 reactions, 27 species), and Scheme 4 by Yu et al. [43] (286 reactions, 34 species).

2.3 Verification of a NO_x Prediction Model

To validate the calculated results against experimental nitrogen oxide emissions data from the UGT3000 gas turbine combustion chamber [36], a reactor-based model specific to this chamber was employed. The burner of the UGT3000 is configured to sustain a near-optimal air-fuel mixture across its entire operating range.

Fuel is introduced through two separate channels. From the first channel, fuel enters the gas cavity of its swirl generator and is then injected through perforations in the vane walls into the inter-vane passages, where initial mixing with air occurs. A similar process takes place in the second channel.

The operational parameters for both the experiment and simulation varied, with the power turbine outlet temperature and the global air excess coefficient (α) ranging from 590 K (α = 3.37) to 915 K (α = 3.20). The combustion chamber pressure was maintained at its nominal value near 1.7 MPa. In the numerical simulation, the two fuel channels were modeled as distinct Perfectly Stirred Reactors (PSRs). These reactors represent the initial mixing zones, allowing for different fuel splits between channels while keeping the total fuel input constant. Depending on local conditions, these PSRs either prepared the mixture or initiated the combustion of a very lean mixture. The outflow from these initial reactors was combined and fed into two larger, serially-connected PSRs, which modeled the primary combustion zone. The subsequent dilution/mixing section of the chamber was represented by two Plug Flow Reactors, where additional air was introduced to cool the combustion products.

Fig. 3 presents a comparison of the computed and experimental data, showing the relationship between the high-pressure compressor speed (n_{HPC}), the fuel mass flow rate (G_f), and the NO_x concentration (C).

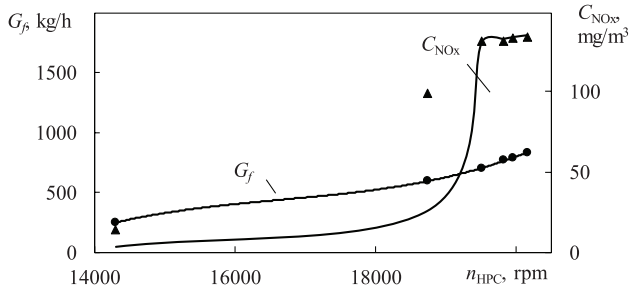

Figure 3: NO_x emissions and fuel flow rate vs. gas turbine operating mode: ▲, •—experimental data; ——calculated results.

The results indicate that NO_x emissions increase with rising n_{HPC} as the engine approaches its nominal power. This trend is attributed to the corresponding increase in gas temperature upstream of the high-pressure turbine, peak combustion zone temperature, and system pressure. The maximum NO_x concentration measured under these conditions was 133 mg/m^3.

Overall, the calculated NO_x emissions are in good agreement with the experimental values. A minor discrepancy observed at the relative engine power mode of $\overline{N}$ = 0.50 is likely due to insufficiently detailed modeling of the mixture formation processes within the flame tube's recirculation zone under these specific transient conditions.

It should be noted that the mathematical model is based on the use of idealized reactors. Therefore, inhomogeneities in mixture formation and the distribution of component concentrations across combustion chamber cross-sections, especially during transient regimes associated with the switching of control and fuel delivery systems, significantly affect the model's predictive capabilities under these transient conditions. This necessitates the use of more complex three-dimensional CFD models that account for the aerodynamic features of the working process as well. However, as can be seen from Fig. 3, satisfactory agreement between measured and calculated results is achieved at the chamber's nominal operating conditions (at high rotational speeds of the high-pressure compressor rotor). Subsequently, our analysis will focus precisely on the nominal operating regimes of the combustion chamber under investigation.

3 Discussion of Results

To analyze the working process in a high-intensity combustion chamber of a gas turbine engine operating on gaseous ammonia, corresponding calculations of fuel combustion in an air environment were performed. The calculations were conducted using the theory of homogeneous and plug-flow reactors with the computational package ANSYS Chemkin [44].

The initial data for the calculations (per single flame tube) were as follows: ammonia mass flow rate at nominal mode 0.255 kg/s, fuel temperature 313 K, air mass flow rate 4.291 (5.1) kg/s without (with) air extraction for turbine blade cooling, air temperature 748 K, air pressure 2.0 MPa, average flame tube diameter 0.165 m, length 0.52 m.

The dependencies of the molar fractions of stable products O_2, H_2O, and N_2, nitrogen oxides NO, N_2O, and NO_2, and the gas temperature at the combustion chamber outlet for the four considered kinetic schemes, as well as their average values, are shown in Fig. 4. It can be seen that, for all the kinetic mechanisms considered, the mole fractions of the major stable species are essentially identical: 0.746 for molecular nitrogen, 0.119 for molecular oxygen, and 0.134 for water vapor, while the temperature of the combustion products at the combustor outlet is 1511 K. This indicates a near-complete agreement between the results of kinetic modeling obtained using different reaction mechanisms with respect to the prediction of stable reaction products. Consequently, the choice of kinetic scheme has a negligible effect on the calculated composition of the main combustion products under the conditions considered.

The main differences are related to the predicted emission characteristics of nitrogen oxides. In particular, kinetic Scheme 4 yields unreasonably high concentrations of nitrous oxide N_2O compared with experimental observations, while simultaneously underestimating the concentration of nitric oxide NO. This behavior suggests limitations in the representation of nitrogen chemistry within Scheme 4, especially in the reaction pathways governing N_2O formation and NO–N_2O interconversion, which reduces its reliability for quantitative NO_x emission prediction under the studied conditions.

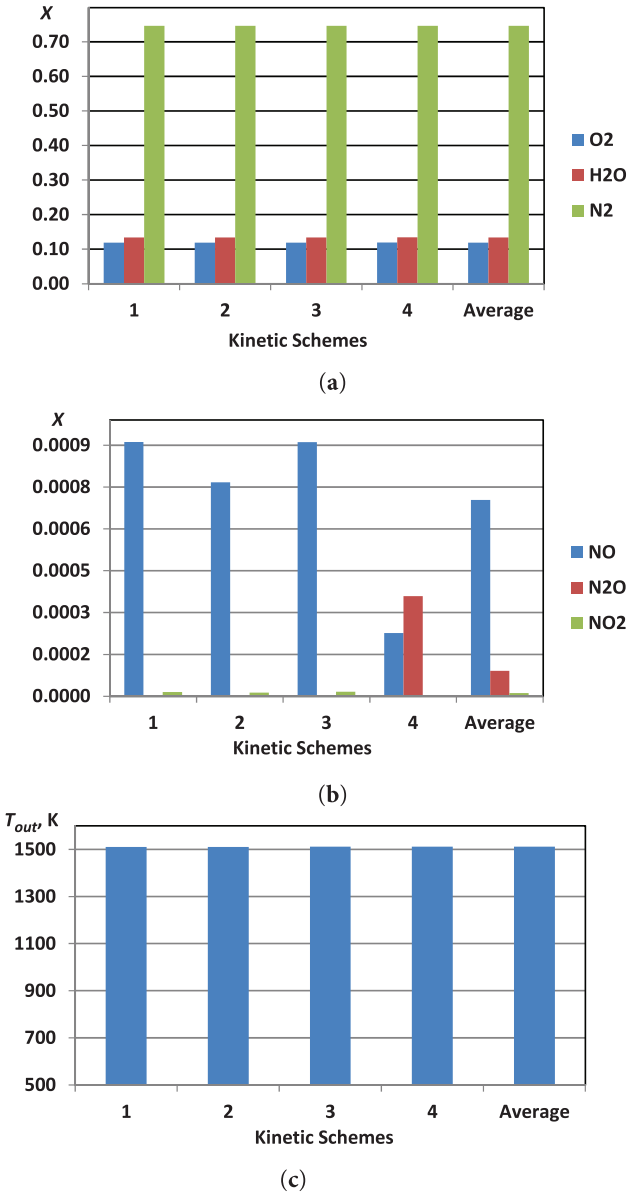

Figure 4: Dependencies of parameters at the combustion chamber outlet for the four kinetic schemes. (**a**) molar fractions of O_2, H_2O, and N_2; (**b**) molar fractions of nitrogen oxides NO, N_2O, and NO_2; (**c**) product temperature.

To identify the patterns of ammonia burnout and toxic component formation in the gas turbine engine combustion chamber, a series of calculations was conducted with ammonia flow rates varying from 0.2 to 0.3 kg/s (per single flame tube), corresponding to a change in the overall air excess coefficient in the chamber from 3.55 to 2.36. The air mass flow rate through the combustion chamber remained unchanged.

Fig. 5 presents the molar fractions of NO, N_2O, NO_2, and volumetric concentrations of NO_x at the combustion chamber outlet as functions of the air excess coefficient for the four considered kinetic schemes. It should be noted that ppmvd (parts per million by volume on a dry basis) 15% O_2 is a unit of gas concentration measurement expressed in parts per million by volume, considering that the measurement is performed on a dry basis (excluding moisture content in the gas mixture) and corrected to a fixed oxygen volume concentration of 15%.

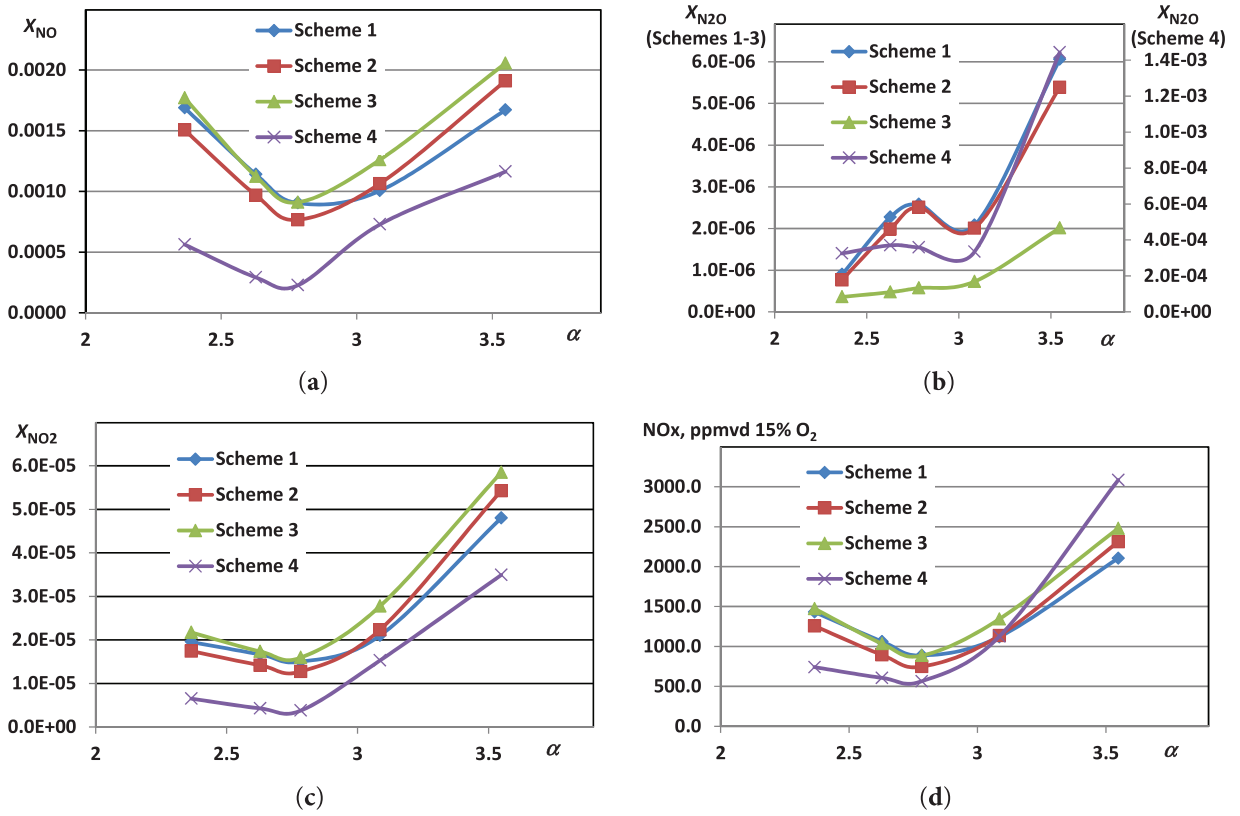

Figure 5: Outlet parameters as a function of the air excess coefficient for the four kinetic schemes. (**a**) molar fractions of NO; (**b**) molar fractions of N_2O; (**c**) molar fractions of NO_2; (**d**) volumetric concentrations of NO_x.

It can be observed that for all considered kinetic schemes, the minimum NO_x emissions occur at a total air excess coefficient of 2.78, corresponding to an average gas temperature of 1511 K before the high-pressure turbine. The total emissions of nitrogen oxides are largely governed by the formation of nitric oxide NO. For the most favorable operating condition in terms of the excess air ratio 2.78, the molar fractions of NO at the combustor outlet for kinetic schemes 1–3 are 9.04×10^{-4}, 7.67×10^{-4}, and 9.11×10^{-4}, respectively, corresponding to NO_x volumetric concentrations of 887.1, 747.8, and 885.4 ppmvd at 15% O_2. The NO emissions exceed those of NO_2 by more than one order of magnitude and those of N_2O by more than two orders of magnitude. This clearly indicates that, under the considered conditions, the formation of NO is the dominant pathway determining the overall NO_x emissions.

Kinetic scheme 3 provides the widest range of stable combustion chamber operation in terms of the air excess coefficients (without flame extinction), which is crucial for future detailed calculations of the aerodynamic flow structure and ammonia burnout in the combustion chamber using three-dimensional CFD models. Therefore, it is recommended for use in subsequent studies.

The dependencies of the molar fractions of O_2, H_2O, and N_2, volumetric concentrations of nitrogen oxides NO and NO_x, and product temperature at the combustion chamber outlet on ammonia flow rate for kinetic Scheme 3 are shown in Fig. 6.

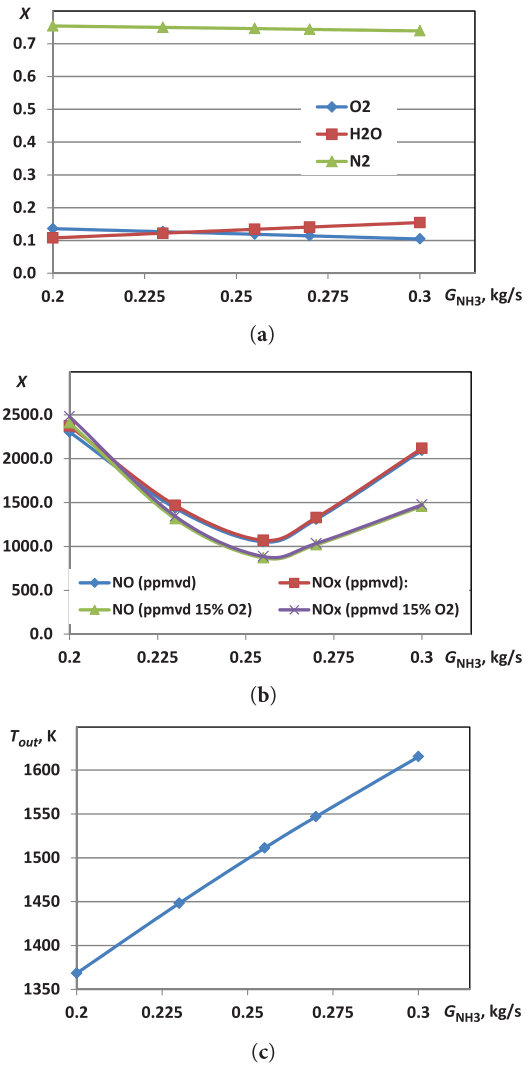

Figure 6: Outlet parameters as a function on ammonia flow rate for kinetic Scheme 3. (**a**) molar fractions of O_2, H_2O, and N_2; (**b**) volumetric concentrations of nitrogen oxides NO and NO_x; (**c**) product temperature.

As the gaseous ammonia flow rate increases, the average gas temperature at the combustion chamber outlet continuously rises. However, NO_x emissions initially decrease, reaching a minimum at a temperature of 1511 K, and then increase. Notably, even under this (calculated) operating mode of the combustion chamber, the NO_x concentration is 885.4 ppmvd 15% O_2, which significantly exceeds the emission levels of gas turbine engines operating on hydrocarbon fuels. Further research is required to optimize the combustion process, primarily by redistributing the air supply across the cross-sections of the flame tube, to reduce nitrogen oxide emissions in such high-intensity combustion chambers with staged air supply.

By redistributing airflow through the swirl vanes (6), the front device (4, 5), and the flame tube (2, 13) by adjusting their passage areas (see Fig. 1), NO_x emissions are expected to be minimized. The combustion process in a gas turbine combustion chamber operating on ammonia was investigated using the detailed chemical combustion mechanism proposed in [39], which includes 160 chemical reactions.

This study proposes an investigation of the impact of air supply configuration on nitrogen oxide formation in a gas turbine combustion chamber for six different cases, each differing in the distribution

of the air excess coefficient along the length of the flame tube. The air distribution along the flame tube corresponds to the supply pattern shown in Fig. 2. A stepwise change in flow rate (as well as the excess air coefficient) occurs for the following sections: air supply through the swirl device, air supply through the front-end device, primary air supply, and secondary air supply. The air flow rate distribution in these sections for all six methods considered is shown in Table 1.

Table 1: The air distribution along the flame tube.

Case	Air flow rate through the swirl device, kg/s	Air flow rate through the front-end device, kg/s	Primary air flow rate, kg/s	Secondary air flow rate, kg/s
1	0.408	0.985	1.257	1.641
2	0.200	1.193	1.257	1.641
3	0.200	0.500	1.950	1.641
4	0.408	0.985	2.098	0.800
5	0.408	0.985	2.748	0.150
6	0.408	0.600	3.133	0.150

The variation of the air excess coefficient along the flame tube length is shown in Fig. 7.

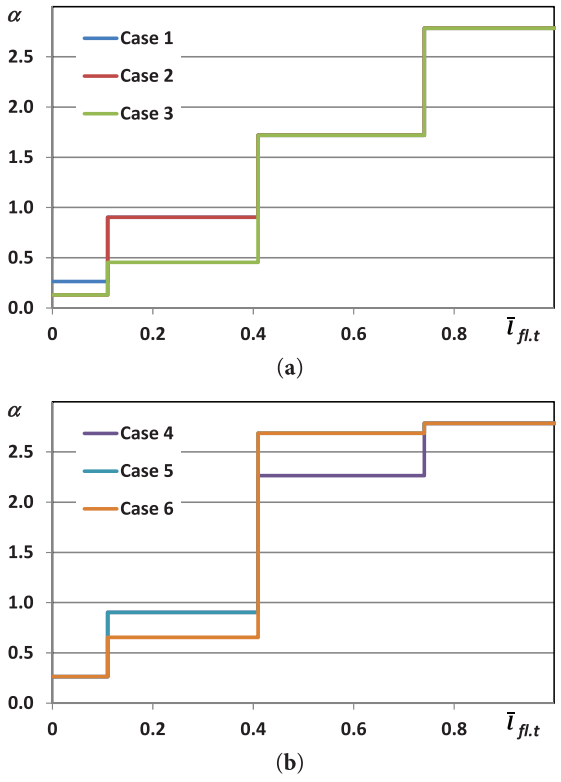

Figure 7: Variation of the air excess coefficient along the flame tube length for the six investigated air distribution. (**a**) Case 1–Case 3; (**b**) Case 4–Case 6.

The distribution of the air excess coefficients is determined by changes in the passage areas of the vane swirlers, two rows of front device holes, as well as the radial holes for primary and secondary air supply

into the flame tube of the combustion chamber. The first three cases involve modifications only in the passage areas of the vane swirler and front device, while the other three cases include additional changes in the passage areas of the primary and secondary air supply holes. It should be noted that Case 1 serves as the baseline configuration, representing the serial design of the flame tube without modifications to the hole areas.

The molar fractions of O_2, H_2O, N_2, NO, N_2O, NO_2, and the volumetric concentrations of NO and NO_x at the chamber outlet for the six air distribution cases studied are shown in Fig. 8.

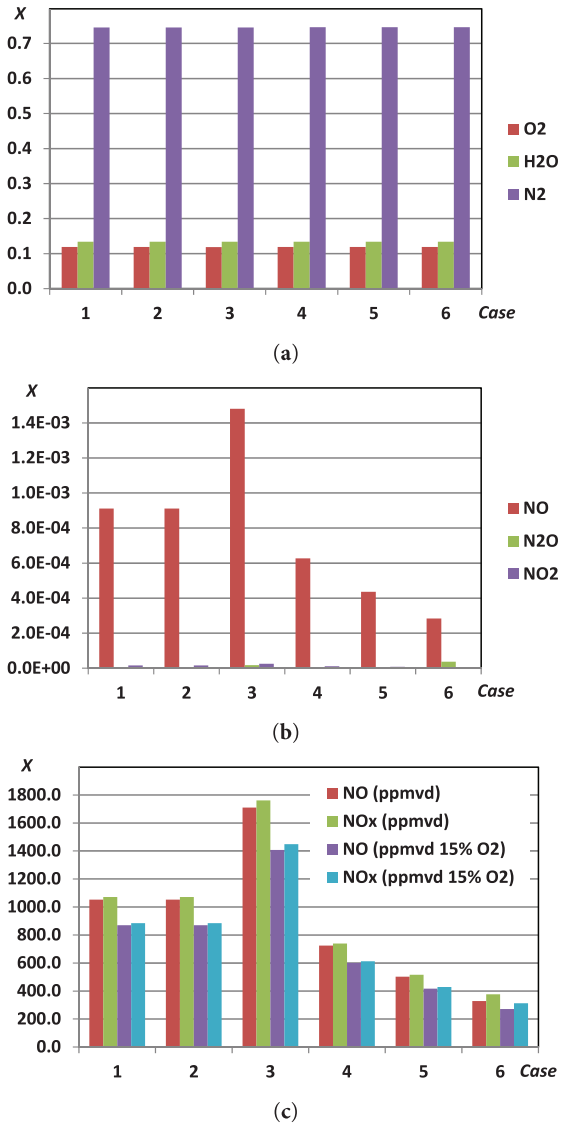

Figure 8: Outlet parameters for the six air distribution options. (**a**) molar fractions of O_2, H_2O, and N_2; (**b**) molar fractions of NO, N_2O, and NO_2; (**c**) volumetric concentrations of NO and NO_x.

The distribution of air along the flame tube length does not affect the concentrations of components such as O_2, H_2O, and N_2 (Fig. 8a) at the combustion chamber outlet but has a significant impact on nitrogen oxide emissions. Based on Fig. 8b, it can be concluded that the primary nitrogen oxide determining the toxicity of

exhaust gases is nitric oxide NO. The highest emissions of this pollutant are characteristic of Case 3, while the lowest emissions correspond to Case 6 (Fig. 8c).

Notably, the sixth (optimized) air distribution case is characterized by a significant increase in the air excess coefficients in the primary air supply zone of the flame tube (at a relative flame tube length of $\bar{l}_{fl.t}$ = 0.41) rising from 0.654 (rich mixture) to 2.686 (lean mixture).

Fig. 9 shows the specific pathways for nitric oxide (NO) formation in the homogeneous reactor HR3 (combustion chamber, see Fig. 2), which is the zone of peak temperature governing primary ammonia consumption. The transformation of fuel-N species here is notably complex, involving a network of competing and consecutive reactions sensitive to local conditions. In particular, the predicted pathways and final NO yield are highly sensitive to the prevailing temperature and to the transient concentrations of unstable intermediates, such as NH_2, NH, and HNO. Normalized sensitivity coefficients for NH_3 in this zone are also provided, along with the key reactions leading to its decomposition and oxidation. This analysis underscores that the combustion chemistry in this critical region is governed by a delicate balance between multiple kinetic paths, which the sensitivity coefficients help to elucidate.

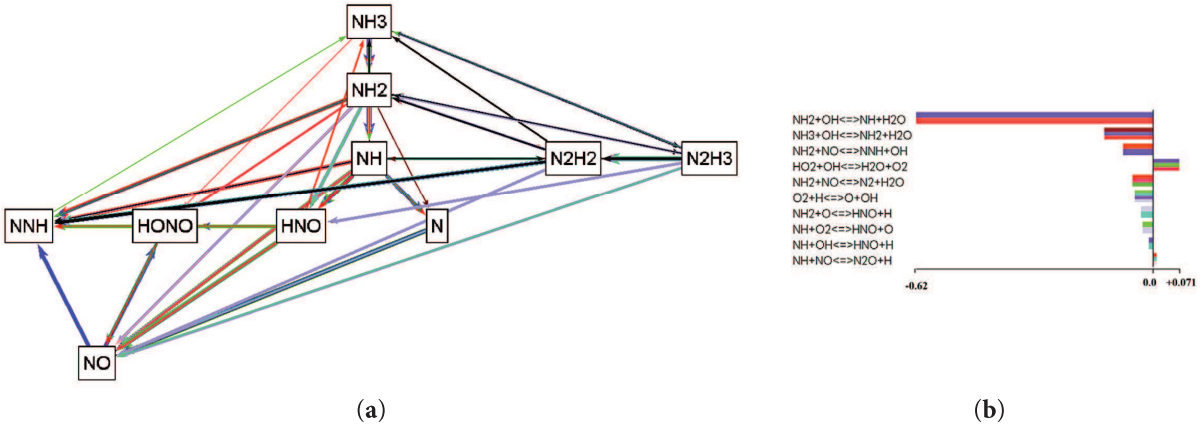

(**a**) (**b**)

Figure 9: Pathways for nitric oxide NO formation within the homogeneous reactor HR3 (**a**) and normalized sensitivity NH_3 (**b**).

The molar fractions of O_2, H_2O, and N_2, volumetric concentrations of NO and NO_x, gas temperature, and molar fraction of ammonia at the chamber outlet, depending on the total excess air coefficient for the case of rational air distribution, are shown in Fig. 10.

As the excess air ratio increases from 2.365 to 3.548, the molar fraction of molecular oxygen rises from 0.105 to 0.137, while the exhaust gas temperature decreases from 1617 to 1370 K. This temperature reduction leads, on the one hand, to a decrease in nitrogen oxide emissions due to their strong temperature dependence. On the other hand, the lower thermal level results in incomplete ammonia burnout within the combustor volume, indicating the necessity for effective combustion enhancement techniques.

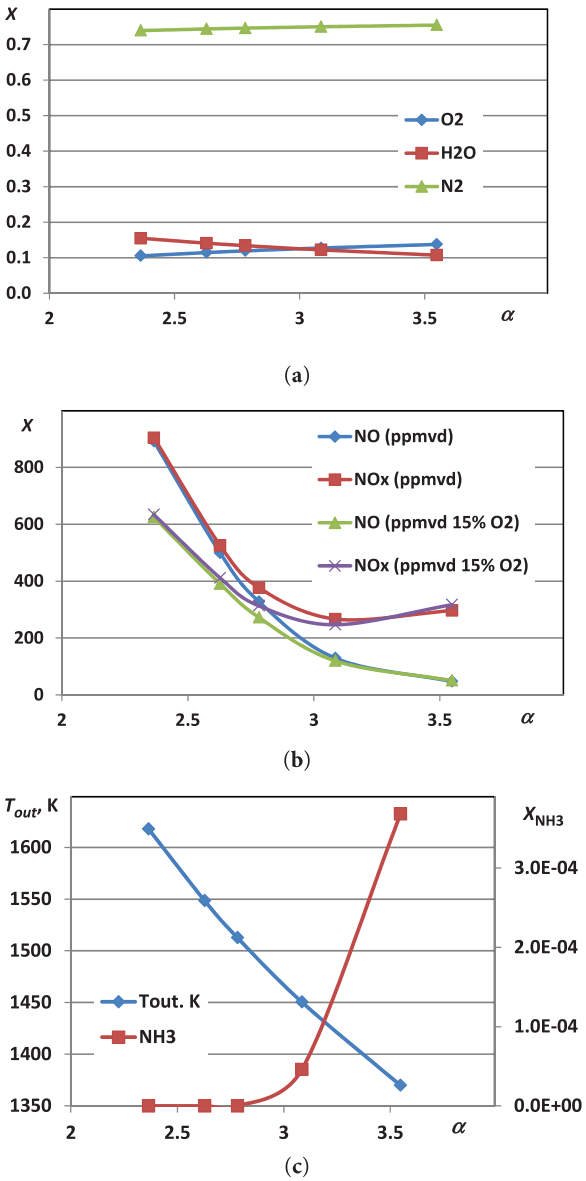

Figure 10: Outlet parameters as a function of the overall air excess coefficient for the optimized air distribution case. (**a**) molar fractions of O_2, H_2O, and N_2; (**b**) volumetric concentrations of NO and NO_x; (**c**) gas temperature and ammonia molar fraction.

It should be noted that, despite the overall decrease in product temperature at excess air ratios above 3, the volumetric concentrations of NO_x exhibit a slight increase. This effect is attributed to the thermal decomposition and oxidation of unburned ammonia in the post-flame region, where residual NH_3 undergoes secondary reactions contributing to additional formation of nitrogen-containing compounds. This behavior highlights the complex trade-off between temperature reduction and chemical completeness in ammonia-fueled combustion systems and underscores the importance of optimized mixing and kinetic control strategies.

Unlike the baseline Case 1, where the volumetric concentration of nitrogen oxides NO_x at the combustion chamber outlet was 885.4 ppmvd at 15% O_2, the concentration in the optimized Case 6 decreased to

312.8 ppmvd at 15% O_2 under the nominal operating conditions (overall air excess coefficient of 2.78, average gas temperature at the outlet of 1512 K).

It should be noted that the efficiency of ammonia combustion can, in many cases, be improved through plasma-assisted intensification [29,31]. In addition, the stable operating range of the combustion chamber can be significantly expanded due to the presence of large quantities of highly reactive intermediate species generated by plasma torches of various types. An undoubted advantage of plasma systems (both equilibrium and non-equilibrium) is the improvement of combustion characteristics during transient modes of power systems, as well as under various natural and climatic conditions, especially during cold start conditions.

This work establishes a methodology for optimizing the design and operation of ammonia-fueled gas turbine combustors. By enabling the minimization of NO_x emissions and guaranteeing complete combustion, it provides essential engineering solutions for retrofitting existing engines and developing new decarbonized propulsion and power systems, thus facilitating the practical use of ammonia as a sustainable zero-carbon fuel.

4 Conclusions

This study employed numerical modeling to investigate the combustion of gaseous ammonia and the formation of nitrogen oxides in a high-intensity gas turbine combustion chamber featuring staged air injection along the flame tube. The primary objective was to identify optimal operating and design parameters for minimizing toxic emissions while ensuring efficient combustion. The main findings are as follows:

(1) A robust mathematical model based on chemical reactor theory and the solution of mass and energy conservation equations was successfully implemented. This model allowed for a detailed analysis of the complex chemical kinetics involved in ammonia combustion and NO_x formation.

(2) The environmental performance of the combustion chamber was evaluated using four detailed ammonia combustion chemical mechanisms (comprising 71 to 286 reactions). This multi-mechanism approach ensured the reliability of the predictions and provided insight into the sensitivity of results to kinetic model selection.

(3) The core finding of this work is the identification of an optimized flame tube configuration with staged air injection. For the studied conditions (pressure of 2.0 MPa, overall excess air ratio ranging from 2.36 to 3.55), this optimized design achieved a substantial reduction in NO_x emissions. The concentration at the chamber outlet was reduced from 885.4 ppmvd at 15% O_2 (baseline configuration) to 312.8 ppmvd at 5% O_2, representing a decrease of approximately 65%. The research established a direct correlation between the staged air distribution pattern, the resulting temperature fields, and the final NO_x yield.

(4) The parametric framework derived from this zero-dimensional analysis provides specific design guidelines (staged air ratios, operational air excess coefficients) for ammonia combustion chambers. To translate these guidelines into a practical prototype, the critical next step is to validate and refine them using three-dimensional CFD simulations. Such modeling is essential to account for turbulent mixing, aerodynamic effects, and three-dimensional flame stabilization, thereby ensuring the predicted emissions reductions are achievable in a real combustor geometry.

Acknowledgement: Not applicable.

Funding Statement: This research was funded by the Ministry of Education and Science of Ukraine (No. 0125U001716).

Author Contributions: The authors confirm contribution to the paper as follows: Conceptualization, Serhiy Serbin; methodology, Serhiy Serbin and Bohdan Lychko; software, Bohdan Lychko and Kateryna Burunsuz; investigation, Serhiy Serbin and Kateryna Burunsuz. All authors reviewed and approved the final version of the manuscript.

Availability of Data and Materials: The data that support the findings of this study are available from the Corresponding Author, [Serhiy Serbin], upon reasonable request.

Ethics Approval: Not applicable.

Conflicts of Interest: The authors declare no conflicts of interest.

References

1. Qi Y, Wang Y, Huang Y. Techno-economic assessment of carbon-neutral ammonia fuel for ships from renewable wind energy. Energies. 2025;18(20):5485. doi:10.3390/en18205485.
2. Pashchenko D. Ammonia fired gas turbines: recent advances and future perspectives. Energy. 2024;290(1):130275. doi:10.1016/j.energy.2024.130275.
3. Tornatore C, Marchitto L, Sabia P, De Joannon M. Ammonia as green fuel in internal combustion engines: state-of-the-art and future perspectives. Front Mech Eng. 2022;8:944201. doi:10.3389/fmech.2022.944201.
4. Eyisse EF, Nadimi E, Wu D. Ammonia combustion: internal combustion engines and gas turbines. Energies. 2024;18(1):29. doi:10.3390/en18010029.
5. Langella G, Sorrentino G, Sabia P, Ariemma GB, Amoresano A, Iodice P. Ammonia as a fuel for gas turbines: perspectives and challenges. J Phys Conf Ser. 2023;2648(1):012009. doi:10.1088/1742-6596/2648/1/012009.
6. Lee H, Lee MJ. Recent advances in ammonia combustion technology in thermal power generation system for carbon emission reduction. Energies. 2021;14(18):5604. doi:10.3390/en14185604.
7. Rocha RC, Costa M, Bai XS. Combustion and emission characteristics of ammonia under conditions relevant to modern gas turbines. Combust Sci Technol. 2021;193(14):2514–33. doi:10.1080/00102202.2020.1748018.
8. Jójka J, Ślefarski R. Emission characteristics for swirl methane—air premixed flames with ammonia addition. Energies. 2021;14(3):662. doi:10.3390/en14030662.
9. Yang R, Liu Z, Liu J. The methodology of decoupling fuel and thermal nitrogen oxides in multi-dimensional computational fluid dynamics combustion simulation of ammonia-hydrogen spark ignition engines. Int J Hydrogen Energy. 2024;55:300–18. doi:10.1016/j.ijhydene.2023.09.105.
10. Yan Y, Yang R, Liu Z, Liu J. Nitrogen oxides emission characteristics of zero-carbon ammonia-hydrogen fuels for internal combustion engines. Detroit, MI, USA: SAE International; 2023. Report No.: 2023-01-0334. doi: 10.4271/2023-01-0334.
11. Liu J, Liu Z. In-cylinder thermochemical fuel reforming for high efficiency in ammonia spark-ignited engines through hydrogen generation from fuel-rich operations. Int J Hydrogen Energy. 2024;54:837–48. doi:10.1016/j.ijhydene.2023.08.146.
12. Yan Y, Liu Z, Liu J. An evaluation of the conversion of gasoline and natural gas spark ignition engines to ammonia/hydrogen operation from the perspective of laminar flame speed. J Energy Resour Technol. 2023;145(1):012302. doi:10.1115/1.4054754.
13. Yan Y, Shang T, Li L, Liu Z, Liu J. Assessing hydrogen—ammonia ratios to achieve rapid kernel inception in spark-ignition engines. J Energy Resour Technol. 2024;146(6):062301. doi:10.1115/1.4065198.
14. Valera-Medina A, Gutesa M, Xiao H, Pugh D, Giles A, Goktepe B, et al. Premixed ammonia/hydrogen swirl combustion under rich fuel conditions for gas turbines operation. Int J Hydrogen Energy. 2019;44(16):8615–26. doi:10.1016/j.ijhydene.2019.02.041.
15. Stagni A, Cavallotti C, Arunthanayothin S, Song Y, Herbinet O, Battin-Leclerc F, et al. An experimental, theoretical and kinetic-modeling study of the gas-phase oxidation of ammonia. React Chem Eng. 2020;5(4):696–711. doi:10.1039/c9re00429g.
16. Kobayashi H, Hayakawa A, Somarathne KDKA, Okafor EC. Science and technology of ammonia combustion. Proc Combust Inst. 2019;37(1):109–33. doi:10.1016/j.proci.2018.09.029.

17. Mathieu O, Petersen EL. Experimental and modeling study on the high-temperature oxidation of ammonia and related NOx chemistry. Combust Flame. 2015;162(3):554–70. doi:10.1016/j.combustflame.2014.08.022.
18. Gobbato P, Masi M, Toffolo A, Lazzaretto A, Tanzini G. Calculation of the flow field and NO_x emissions of a gas turbine combustor by a coarse computational fluid dynamics model. Energy. 2012;45(1):445–55. doi:10.1016/j.energy.2011.12.013.
19. Okafor EC, Somarathne KDKA, Hayakawa A, Kudo T, Kurata O, Iki N, et al. Towards the development of an efficient low-NOx ammonia combustor for a micro gas turbine. Proc Combust Inst. 2019;37(4):4597–606. doi:10.1016/j.proci.2018.07.083.
20. Mohammed AG, Mansyur N, Hasini H, Elfeky KE, Wang Q, Ali MH, et al. Review on the ammonia-blend as an alternative fuel for micro gas turbine power generation. Int J Hydrogen Energy. 2024;82:428–47. doi:10.1016/j.ijhydene.2024.07.396.
21. Okafor EC, Kurata O, Yamashita H, Inoue T, Tsujimura T, Iki N, et al. Liquid ammonia spray combustion in two-stage micro gas turbine combustors at 0.25 MPa; relevance of combustion enhancement to flame stability and NOx control. Appl Energy Combust Sci. 2021;7(2):100038. doi:10.1016/j.jaecs.2021.100038.
22. Kurata O, Iki N, Inoue T, Matsunuma T, Tsujimura T, Furutani H, et al. Development of a wide range-operable, rich-lean low-NOx combustor for NH_3 fuel gas-turbine power generation. Proc Combust Inst. 2019;37(4):4587–95. doi:10.1016/j.proci.2018.09.012.
23. Ditaranto M, Saanum I, Larfeldt J. Experimental study on high pressure combustion of decomposed ammonia: how can ammonia be best used in a gas turbine? In: Proceedings of the ASME Turbo Expo 2021: Turbomachinery Technical Conference and Exposition; 2021 Jun 7–11; Virtual. New York, NY, USA: ASME; 2021. doi:10.1115/gt2021-60057.
24. Matveev IB, Serbin SI, Wolf K. Plasma-assisted ammonia combustion: part 1: possibilities of plasma combustion of ammonia in air and oxygen. IEEE Trans Plasma Sci. 2023;51(6):1446–50. doi:10.1109/TPS.2023.3273462.
25. Cai T, Tang A, Zhang Q, Ni Q, Li J. A systematic review of enhancing stabilization performance and mitigating thermoacoustic instability in renewable ammonia turbulent combustion. Renew Sustain Energy Rev. 2025;217:115760. doi:10.1016/j.rser.2025.115760.
26. Cai T, Chen K, Tang A. Insights into ignition, flame propagation, and emission characteristics of ammonia/hydrogen combustion under intermediate-to-high temperatures and high pressures. Chem Eng J. 2025;526:171040. doi:10.1016/j.cej.2025.171040.
27. Wang P, Liu W, Qian W, Cheng K, Wang Y, Roy S. Investigation of no emission characteristic of ammonia-hydrogen flame in a two-stage model combustor. Therm Sci. 2024;28(2 Pt C):1689–99. doi:10.2298/tsci230428199w.
28. Matveev IB, Serbin SI. Plasma-assisted ammonia combustion: part 3: combustion of ammonia in air. IEEE Trans Plasma Sci. 2024;52(4):1157–61. doi:10.1109/TPS.2023.3343389.
29. Matveev IB, Serbin SI. Theoretical and experimental investigations of the plasma-assisted combustion and reformation system. IEEE Trans Plasma Sci. 2010;38(12):3306–12. doi:10.1109/TPS.2010.2063713.
30. Matveev IB, Tropina AA, Serbin SI, Kostyuk VY. Arc modeling in a plasmatron channel. IEEE Trans Plasma Sci. 2008;36(1):293–8. doi:10.1109/TPS.2007.913876.
31. Serbin SI, Matveev IB, Goncharova NA. Plasma-assisted reforming of natural gas for GTL: part I. IEEE Trans Plasma Sci. 2014;42(12):3896–900. doi:10.1109/TPS.2014.2353042.
32. Matveev I, Serbin S, Butcher T, Tutu N. Flow structure investigations in a "tornado" combustor. In: 4th International Energy Conversion Engineering Conference and Exhibit (IECEC); 2006 Jun 26–29; San Diego, CA, USA. doi:10.2514/6.2006-4141.
33. Sekiguchi H. Experimental investigations of plasma-assisted ammonia combustion using rod-electrode-type microwave plasma source. Int J Hydrogen Energy. 2024;65:66–73. doi:10.1016/j.ijhydene.2024.03.370.
34. Fichet V, Kanniche M, Plion P, Gicquel O. A reactor network model for predicting NOx emissions in gas turbines. Fuel. 2010;89(9):2202–10. doi:10.1016/j.fuel.2010.02.010.
35. Grimm F. Low-order reactor-network-based prediction of pollutant emissions applied to FLOX® combustion. Energies. 2022;15(5):1740. doi:10.3390/en15051740.

36. Movchan SN, Romanov VV, Chobenko VN, Shevtsov AP. Contact steam-and-gas turbine units of the "AQUARIUS" type: the present status and future prospects. In: ASME Turbo Expo 2009: Power for Land, Sea, and Air; 2009 Jun 8–12; Orlando, FL, USA. p. 703–9. doi:10.1115/GT2009-60339.
37. Kee RJ, Miller JA. A structured approach to the computational modeling of chemical kinetics and molecular transport in flowing systems. Albuquerque, NM, USA: Sandia National Laboratories; 1988.
38. Sandu A, Daescu DN, Carmichael GR. Direct and adjoint sensitivity analysis of chemical kinetic systems with KPP: part I—theory and software tools. Atmos Environ. 2003;37(36):5083–96. doi:10.1016/j.atmosenv.2003.08.019.
39. Chen D, Serbin S, Burunsuz K. Features of a gas turbine combustion chamber in operation with gaseous ammonia. Fuel. 2024;372(1):132149. doi:10.1016/j.fuel.2024.132149.
40. Xiao H, Valera-Medina A, Bowen PJ. Modeling combustion of ammonia/hydrogen fuel blends under gas turbine conditions. Energy Fuels. 2017;31(8):8631–42. doi:10.1021/acs.energyfuels.7b00709.
41. Stagni A, Arunthanayothin S, Dehue M, Herbinet O, Battin-Leclerc F, Bréquigny P, et al. Low- and intermediate-temperature ammonia/hydrogen oxidation in a flow reactor: experiments and a wide-range kinetic modeling. Chem Eng J. 2023;471:144577. doi:10.1016/j.cej.2023.144577.
42. Li Y, Jin Z, Wang Z, Tan H, Jia Z, Cui B, et al. Evaluation, reduction, and validation of a new skeletal mechanism for the cofiring of NH_3 and CH_4. ACS Omega. 2023;8(49):47113–22. doi:10.1021/acsomega.3c07094.
43. Yu Z, Li X, Zhao J, Shi L. Development of ammonia reaction kinetic mechanism under engine-relevant conditions. Energy Fuels. 2024;38(1):728–41. doi:10.1021/acs.energyfuels.3c03241.
44. Kee RJ, Rupley FM, Miller JA. Chemkin-II: a Fortran chemical kinetics package for the analysis of gas phase chemical kinetics. Oak Ridge, TN, USA: Office of Scientific and Technical Information; 1989. Report No.: SAND89-8009B. doi:10.2172/5681118.